DOI:
10.1242/dev.181933

Document Version
Publisher's PDF, also known as Version of record

© 2019. Published by The Company of Biologists Ltd | Development (2019) 146, dev181933. doi:10.1242/dev.181933

STEM CELLS AND REGENERATION

RESEARCH ARTICLE

The p75 neurotrophin receptor is required for the survival of neuronal progenitors and normal formation of the basal forebrain, striatum, thalamus and neocortex

Sonja Meier[1,*], Fabienne Alfonsi[1,*], Nyoman D. Kurniawan[2], Michael R. Milne[3], Maria A. Kasherman[4], Alessio Delogu[5], Michael Piper[1] and Elizabeth J. Coulson[1,3,‡]

ABSTRACT

During development, the p75 neurotrophin receptor ($p75^{NTR}$) is widely expressed in the nervous system where it regulates neuronal differentiation, migration and axonal outgrowth. $p75^{NTR}$ also mediates the survival and death of newly born neurons, with functional outcomes being dependent on both timing and cellular context. Here, we show that knockout of $p75^{NTR}$ from embryonic day 10 (E10) in neural progenitors using a conditional Nestin-Cre $p75^{NTR}$ floxed mouse causes increased apoptosis of progenitor cells. By E14.5, the number of Tbr2-positive progenitor cells was significantly reduced and the rate of neurogenesis was halved. Furthermore, in adult knockout mice, there were fewer cortical pyramidal neurons, interneurons, cholinergic basal forebrain neurons and striatal neurons, corresponding to a relative reduction in volume of these structures. Thalamic midline fusion during early postnatal development was also impaired in Nestin-Cre $p75^{NTR}$ floxed mice, indicating a novel role for $p75^{NTR}$ in the formation of this structure. The phenotype of this strain demonstrates that $p75^{NTR}$ regulates multiple aspects of brain development, including cortical progenitor cell survival, and that expression during early neurogenesis is required for appropriate formation of telencephalic structures.

KEY WORDS: Brain development, Cortical development, Neuronal progenitor survival, Thalamic midline fusion, P75 knockout mouse, P75 neurotrophin receptor

INTRODUCTION

Formation of the central nervous system, where uncommitted stem cells give rise to neural precursors that then differentiate into mature neurons, is governed by the interaction between intrinsic genetic programs and extrinsic cues such as growth factors. Among these cues is the neurotrophin family of secreted growth factors, which regulate the generation, migration, maturation and survival of neurons (Reichardt, 2006). The broad spectrum of biological activities exerted by these proteins is due to their ability to bind the tyrosine kinase (Trk) receptors and the common neurotrophin receptor, $p75^{NTR}$. While association of the $p75^{NTR}$ with Trk receptors in response to mature neurotrophin binding is associated with trophic signaling, including neurite outgrowth and neuronal survival, it is well known that $p75^{NTR}$ can also induce cell death and neurite pruning in some situations by binding pro-neurotrophins that induce apoptosis in combination with sortilin receptors (Ibáñez and Simi, 2012).

During development, the role of $p75^{NTR}$ has primarily been characterized as mediating the survival or developmental programmed cell death of newly born neurons. However, $p75^{NTR}$ can also regulate aspects of neurogenesis. Previously, we reported that $p75^{NTR}$ is expressed by neurogenic stem cells in the postnatal and adult rodent ventricular/subventricular zone, which supply the rostral migratory stream and olfactory bulb (Young et al., 2007). Activation of $p75^{NTR}$ in these cells causes their differentiation into neurons. $p75^{NTR}$ deficiency also affects adult hippocampal neurogenesis, although whether this effect is direct or indirect remains unclear (Bernabeu and Longo, 2010; Catts et al., 2008; Colditz et al., 2010). In addition, $p75^{NTR}$-mediated signals have been shown to regulate the proliferation and differentiation of neural and non-neural cells *in vitro* (Cattaneo and McKay, 1990; Chittka and Chao, 1999; Erck et al., 1998) and *in vivo*, including promoting the cell-cycle exit and differentiation of cerebellar granule neurons during the development of the cerebellum (Zanin et al., 2016). Surprisingly, however, the role of $p75^{NTR}$ in cortical neurogenesis during development remains unclear.

As the functional outcome of $p75^{NTR}$ signaling is highly dependent on cellular context, we examined the *in vivo* effect of conditional $p75^{NTR}$ gene deletion from neural precursors from embryonic day (E) 10.5 using our $p75^{NTR}$ floxed mouse strain (Boskovic et al., 2014) crossed to a Nestin-Cre deleter line. Here, we report that knockout of $p75^{NTR}$ in neural progenitor cells during telencephalic development causes an increased rate of apoptosis of both pyramidal and GABAergic cortical neuron progenitors, resulting in a disproportionally thinner cortex, as well as a reduced number of cholinergic basal forebrain and striatal neurons. Loss of $p75^{NTR}$ also prevented the correct formation of the thalamus postnatally, revealing a novel function for $p75^{NTR}$ in thalamic midline fusion during early postnatal development.

RESULTS

The p75 neurotrophin receptor is expressed transiently in newly born neurons during brain development

We first analyzed $p75^{NTR}$ expression at different stages of development by immunohistochemical staining of embryonic mouse brain sections. $p75^{NTR}$ protein could be detected as early as E11.5,

[1]Queensland Brain Institute, The University of Queensland, 4072 Brisbane, Australia. [2]Centre for Advanced Imaging, The University of Queensland, 4072 Brisbane, Australia. [3]School of Biomedical Sciences, The University of Queensland, 4072 Brisbane, Australia. [4]Griffith Institute for Drug Discovery, Griffith University, 4122 Brisbane, Australia. [5]Department of Basic and Clinical Neuroscience, Institute of Psychiatry, Psychology and Neuroscience, Kings College, London SE5 9RX, UK.
*These authors contributed equally to this work

‡Author for correspondence (e.coulson@uq.edu.au)

S.M., 0000-0001-7001-0819; N.D.K., 0000-0001-6340-182X; M.R.M., 0000-0002-4716-8316; M.A.K., 0000-0003-0169-7578; A.D., 0000-0002-4414-4714; M.P., 0000-0002-6759-2560; E.J.C., 0000-0003-3783-6197

Received 25 June 2019; Accepted 19 August 2019

Development (2019) 146, dev181933. doi:10.1242/dev.181933

when expression became visible in the ventral part of the telencephalon (Fig. 1A), and with the protein being predominantly expressed in βIII tubulin-positive cells that had migrated out of the proliferative zones. Expression in the ventral telencephalon increased throughout the early stages of development as neurons were born. $p75^{NTR}$ expression was detected in postmitotic neurons in the cortex at E13.5, and at E14.5 it was present in radially projecting neurons of the cortical plate and in migrating neurons within the intermediate zone. From E16.5, $p75^{NTR}$ expression in the ventral telencephalon decreased coincident with the disappearance of the transient ganglionic eminences, with the exception of a ventrolaterally localized neuronal population in which $p75^{NTR}$ expression continued in fibers projecting laterally to the cortex, and the presumptive basal forebrain.

To study the effect of $p75^{NTR}$ in the cells of the developing brain, our conditional $p75^{NTR}$ knockout mouse strain ($p75^{fl/fl}$; Boskovic et al., 2014) was crossed to a Nestin-Cre deleter line (Nestin-Cre; Dubois et al., 2006). Nestin is expressed in progenitor cells of the neuronal lineage and Nestin-Cre-driven recombination is observed from around E10.5 onward (Dubois et al., 2006), resulting in knockout of $p75^{NTR}$ in progenitor cells of the neuronal lineage from early embryogenesis. The efficiency of the knockout was assessed by staining for the marker mCherry in embryonic brain sections at E12.5 and E14.5 (Fig. 1B).

The brain volume of Nestin-Cre $p75^{in/in}$ is decreased and the neocortex and basal ganglia are disproportionally reduced

Nestin-Cre $p75^{in/in}$ mice were born in the expected Mendelian ratio and equal sex ratio (Fig. S1A,B). However, these mice were noticeably smaller than their $p75^{fl/fl}$ littermates (Fig. 2A; Fig. S1C,D) and animals of the Nestin-Cre parental strain (Fig. S1D). However, no overt motor or behavioral differences were observed (Fig. S2) and adult mice were fertile. Histological analysis of adult Nestin-Cre $p75^{in/in}$ mice revealed a significantly decreased brain volume, with a decrease in the thickness of the cortex (−29%) and the volume of the caudate putamen (−42%) compared with control $p75^{fl/fl}$ animals (Fig. 2B,C) and those from the Nestin-Cre single line (Fig. S3). As expected, $p75^{NTR}$ protein expression was undetectable in the basal forebrain of the adult Nestin-Cre $p75^{in/in}$ animals, confirming the success of the knockout strategy in neuronal cells (data not shown; see Boskovic et al., 2014).

In order to characterize the altered brain architecture and accurately measure the brain volume of the Nestin-Cre $p75^{in/in}$ mice, three-dimensional images of knockout and control brains were acquired by *ex vivo* MRI. The volume of the whole brain and individual areas, including the cerebral cortex, hippocampus, basal forebrain, diencephalon (including the thalamus, epithalamus and hypothalamus) and cerebellum, were measured using registered

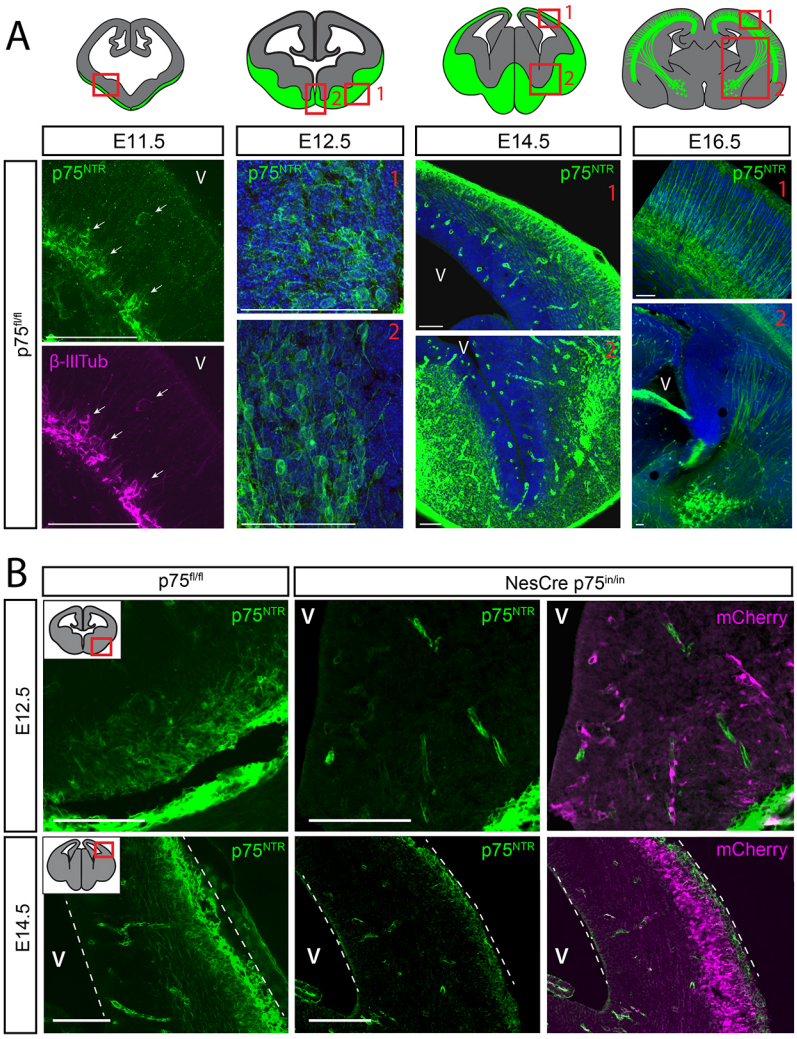

Fig. 1. Spatiotemporal mapping of $p75^{NTR}$ expression in the developing telencephalon. (A) Schematic representations of coronal embryonic mouse brain sections from E11.5 to E16.5 and corresponding immunostaining for $p75^{NTR}$ and βIII tubulin (E11.5). Arrows indicate the same cell co-stained for both markers. Scale bars: 100 µm. (B) Representative images of E12.5 and E14.5 brain sections of control ($p75^{fl/fl}$) embryos stained for $p75^{NTR}$ and knockout (NesCre $p75^{in/in}$) embryos stained for $p75^{NTR}$ and mCherry, qualitatively illustrating the knockout efficiency. Scale bars: 200 µm. V, ventricle.

Development (2019) 146, dev181933. doi:10.1242/dev.181933

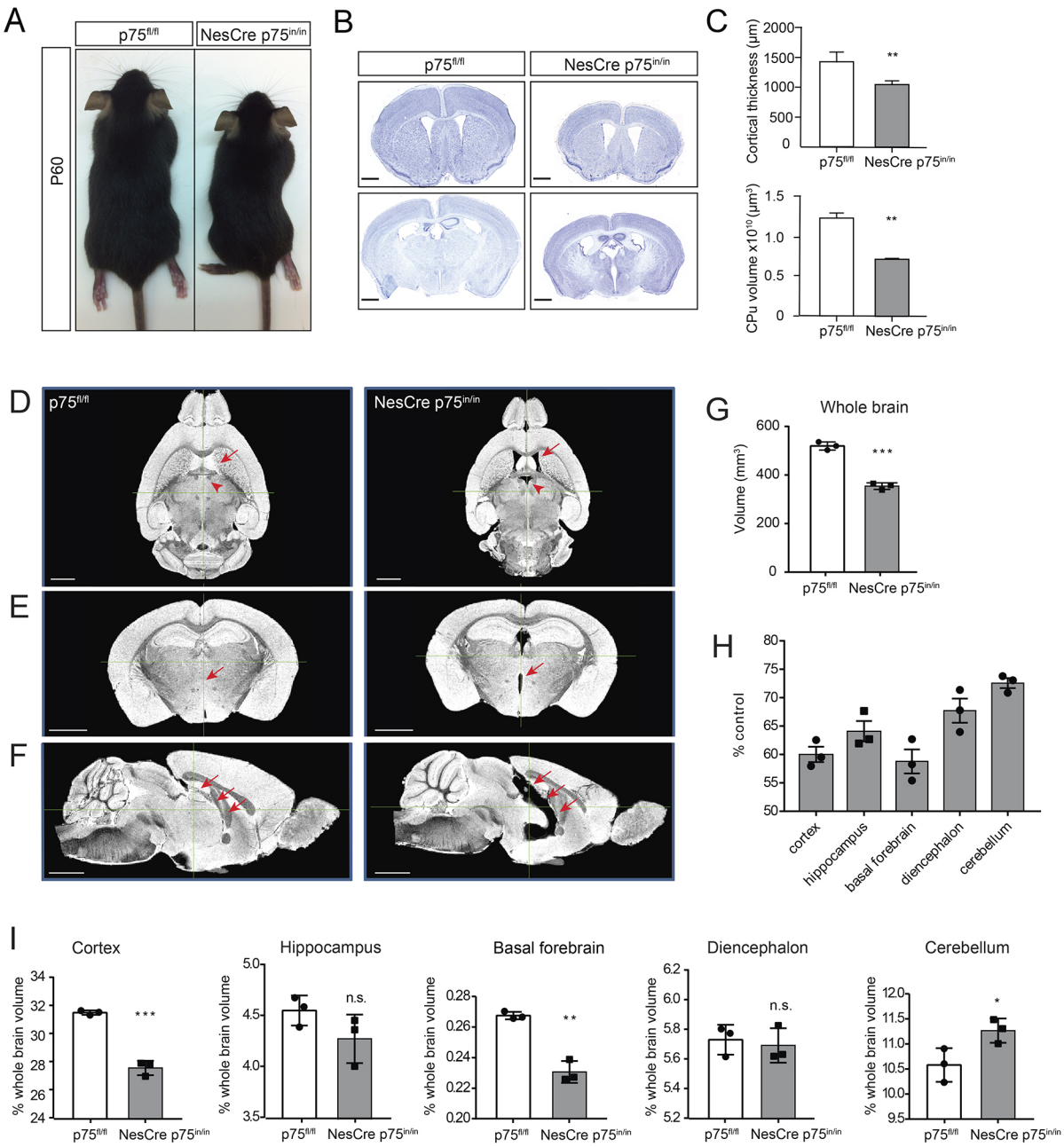

Fig. 2. Nestin-Cre (NesCre) p75$^{in/in}$ mice show reduced growth and have smaller brain volume. (A) Images of a control (p75$^{fl/fl}$) and knockout (NesCre p75$^{in/in}$) mouse at P60 depicting the difference in size. (B) Nissl staining of control (p75$^{fl/fl}$) and knockout (NesCre p75$^{in/in}$) mouse coronal brain sections illustrating reduced brain size and altered structures of the knockout mice. Scale bars: 1 mm. (C) Quantification of cortical thickness and the volume of the caudate putamen (CPu) from histological sections (n=4 brains per genotype; mean±s.e.m.). Student's t-test. (D-F) MRI contrast images illustrating the atrophic brain structure and enlarged ventricles in a NesCre p75$^{in/in}$ mouse compared with a control mouse at 3 months of age. Scale bars: 2 mm. (D) Axial view comparing the 4th ventricle (arrowhead) and lateral ventricles (arrow) in NesCre p75$^{in/in}$ and control mice. (E) Coronal view highlighting the thalamic fissure (arrow) present in a NesCre p75$^{in/in}$ mouse. (F) Sagittal view showing tissue reduction and large internal cavity (arrows) in a NesCre p75$^{in/in}$ mouse. (G) Quantification of the whole-brain volume of control and NesCre p75$^{in/in}$ mice. (H) Reduction in volumes of individual brain regions in NesCre p75$^{in/in}$ mice as a percentage of controls. (I) Volume of individual brain regions normalized to whole-brain volume showing relative change compared with control. n=3 mice per genotype, data are mean ±s.e.m., Student's t-test. *P<0.05, **P<0.01, ***P<0.001; n.s., not significant.

C57/BL6 MRI atlases. Analysis of MRI imaging revealed structural abnormalities in the brain of adult p75^{NTR} knockout animals, including dilated lateral and 4th ventricles, and a thalamic fissure along the midline, that were not present in control mice (Fig. 2D-F). Consistent with the results of histological analyses, the volumetric measurements revealed that the whole-brain volume was significantly reduced in Nestin-Cre p75$^{in/in}$ animals compared with controls (−31.9±2.2%; Fig. 2G). The subregions were also reduced in volume, although to varying extents (Fig. 2H). The neocortex and basal forebrain were the most severely affected, with a reduction of 40.0±2.2% and 41.2±3.6%, respectively, whereas the cerebellum was found to be only 27.4±1.2% smaller than in control animals. Given that Nestin-Cre p75$^{in/in}$ mice were stunted in growth, the volumes of the measured brain areas were normalized to the

Development (2019) 146, dev181933. doi:10.1242/dev.181933

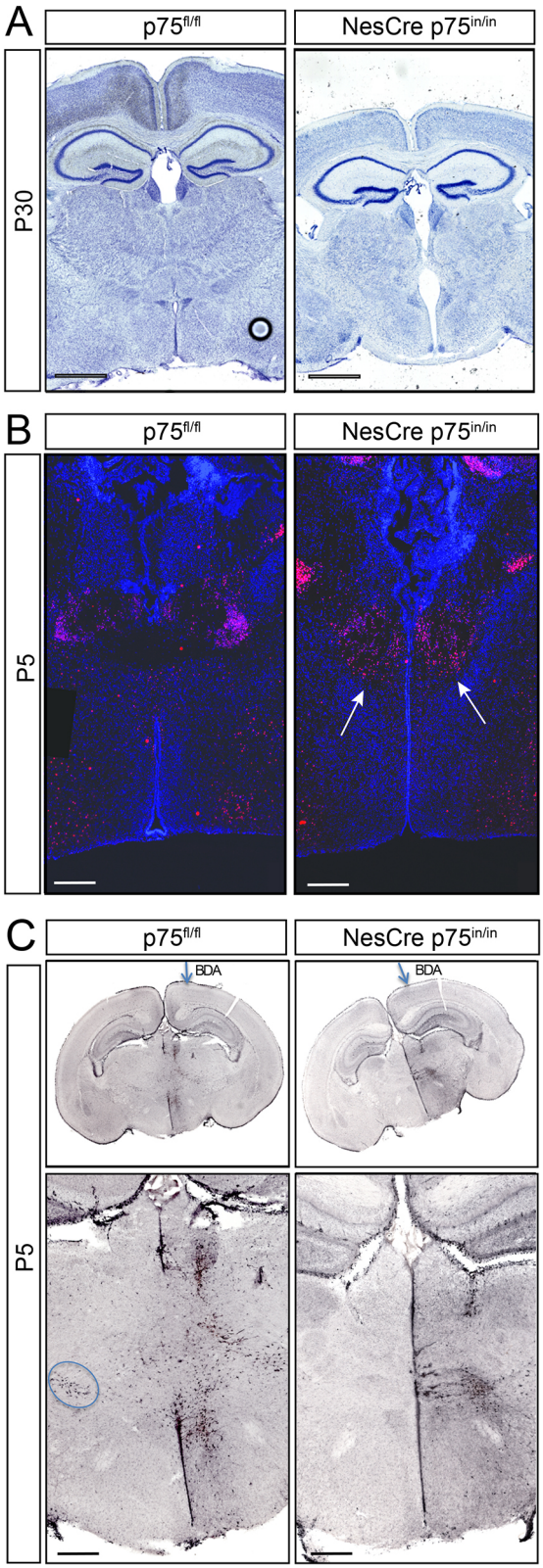

Fig. 3. Impaired thalamic midline fusion in postnatal Nestin-Cre (NesCre) p75$^{in/in}$ mice. (A) Nissl staining of adult coronal mouse brain sections showing the thalamic fissure present in NesCre p75$^{in/in}$ mice. Scale bars: 1 mm. (B) Immunostaining for Tbr1 (red) and the nuclear marker DAPI (blue) in coronal brain sections of control (p75$^{fl/fl}$) and knockout (NesCre p75$^{in/in}$) mice. Scale bars: 400 µm. Arrows indicate accumulating Tbr1-positive cells on either side of the midline. (C) Streptavidin-coupled horseradish peroxidase staining of biotinylated dextran-amine (BDA) in coronal thalamic sections of P5 control (p75$^{fl/fl}$) and knockout (NesCre p75$^{in/in}$) mice. The BDA was injected into the right hemisphere of P3 animals (arrow). Scale bars: 400 µm. The circle indicates biotin-positive cells that had migrated across the midline in control animals but were absent in images of NesCre p75$^{in/in}$ mice. *n*=5 mice per genotype for all analyses.

whole-brain volume (Fig. 2I). This revealed that the volumes of the neocortex and the basal forebrain of knockout mice were disproportionately smaller relative to the entire brain, whereas the cerebellum, despite being smaller than the control, was proportionally larger when measured against the entire brain. The difference in severity of the affected brain areas likely reflects different roles of p75^{NTR} in the development of each structure.

p75^{NTR} is required for postnatal thalamic midline closure

Another major change in brain structure in the postnatal Nestin-Cre p75$^{in/in}$ mice was a fissure along the thalamic midline (Fig. 2E; Fig. 3A) and a smaller absolute size of the diencephalon (Fig. 2H). We first assessed gene transcription in the developing thalamus by *in situ* hybridization of the key thalamic developmental markers *Dlx2*, *Ascl1*, *Helt*, *Sox14*, *Lhx9* and *Lhx1* (Andrews et al., 2003; Hashimoto-Torii et al., 2003; Nakagawa and O'Leary, 2001; Song et al., 2015), and analyzed morphological changes by immunohistochemistry. No difference in the transcriptional expression of thalamic developmental markers was observed at E12.5 (Fig. S4), indicating that altered thalamic morphology was unlikely to be due to a failure of cellular specification. The thalamus initially exists as two bilaterally separate structures (Fig. S4) that fuse across the midline to form a single structure around P2 (Takada et al., 1987). Midline fusion permits the thalamic neurons to migrate across the midline in order to acquire contralateral axonal projections. Analysis of P5 embryos revealed that, whereas the thalamic hemispheres in control animals were fused, knockout animals retained unfused hemispheres, with an accumulation of Tbr1-positive neurons observed in each thalamic hemisphere close to the midline (Fig. 3B).

We therefore tested whether thalamic bilateral migration was impaired in Nestin-Cre p75$^{in/in}$ mice by injecting BDA unilaterally into the thalamus of P2 Nestin-Cre p75$^{in/in}$ and p75$^{fl/fl}$ mice. The location of the biotin-positive cells was examined at P5, after midline fusion in control animals was largely complete (Fig. 3C). In control animals, a significant population of biotin-positive cells was found within the contralateral thalamic hemisphere, with accumulation particularly occurring in ventral thalamic nuclei (Fig. 3C). In contrast, biotin-labeled cells in the Nestin-Cre p75$^{in/in}$ animals did not cross the midline but rather accumulated at the unfused midline of the injected hemisphere. These results suggest a novel role for p75^{NTR} in the control of thalamic midline fusion during postnatal development.

p75^{NTR} is required for the development of cortical interneurons and upper-layer pyramidal neurons

To determine the reason for the reduced cortical volume, coronal brain sections of Nestin-Cre p75$^{in/in}$ and littermate control mice were stained using the Golgi-Cox silver method. Low-resolution images suggested a reduced number and disorganization of pyramidal neurons in the upper layers of the cortex (Fig. 4A). The morphology of the pyramidal neurons was also altered (Fig. 4B). Quantification and Sholl analyses of total dendrites, soma size and number of dendritic trees revealed no significant differences

Development (2019) 146, dev181933. doi:10.1242/dev.181933

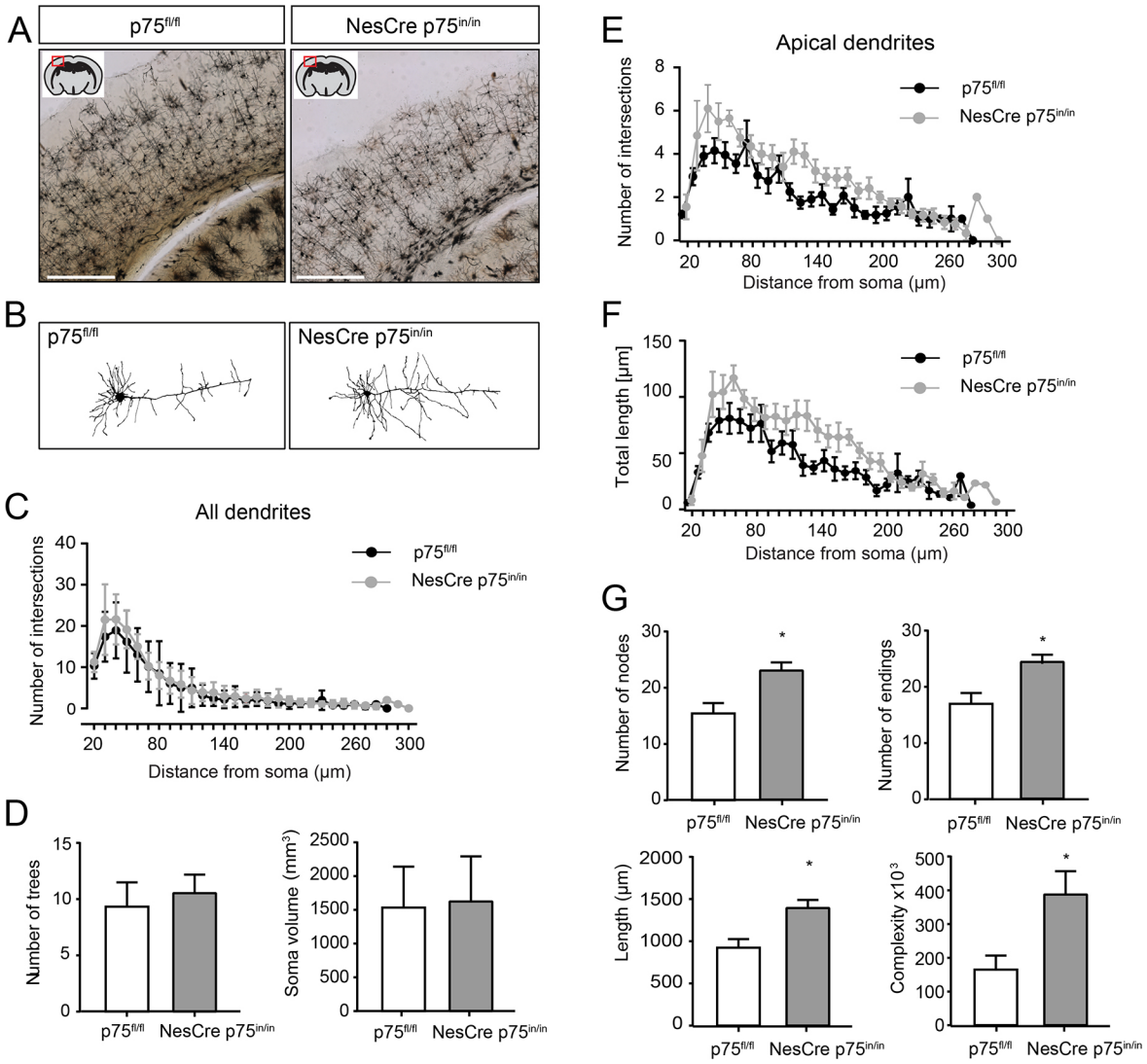

Fig. 4. Golgi silver stain showing changed neuronal morphology in Nestin-Cre (NesCre) p75$^{in/in}$ mice. (A) Low-resolution light microscopy image of a Golgi silver-stained coronal section of the neocortex of adult control (p75$^{fl/fl}$) and knockout (Nestin-Cre p75$^{in/in}$) mice at 6 months of age. Scale bars: 500 µm. (B) Representative tracing images of control (p75$^{fl/fl}$) and knockout (Nestin-Cre p75$^{in/in}$) layer V neurons. (C) Sholl analysis of the number of intersections of total dendritic trees of layer V pyramidal neurons. (D) Quantification of total number of dendritic trees and soma size of layer V pyramidal neurons. (E,F) Sholl analysis of the number of intersections (E) and total length of layer V pyramidal neuron apical dendrites (F). (G) Quantification of number of nodes and endings, complexity (arbitrary values), and total length of layer V pyramidal neuron apical dendrites. *n*=20 (four animals were analyzed, five neurons traced per animal; data are mean±s.e.m.). Sholl analyses were examined using a two-way ANOVA test. An alpha level of 0.05 was considered significant. Significant effects and interactions were further analyzed using the Holm-Sidak's post-hoc multiple comparisons test. Student's *t*-tests were used for comparisons of single parameters between the two groups. *P<0.05.

between genotypes (Fig. 4C,D). However, when analyzed separately, the apical dendrites of layer V neurons in Nestin-Cre p75$^{in/in}$ mice showed increased overall dendritic complexity compared with those of p75$^{fl/fl}$ mice, displaying longer total dendritic length (+50.3 ±7.3%), and a higher total number of dendritic nodes (+48.5±10.7%) and endings (+43.3±10.3%; Fig. 4E-G). Nonetheless, these results suggested that a reduction in cell number rather than cell complexity may be the primary reason for the reduction in cortical volume in Nestin-Cre p75$^{in/in}$ mice.

Next, we investigated whether the six-layered neocortical laminar architecture in the primary somatosensory cortex was affected in p75^{NTR} knockout mice. p75$^{fl/fl}$ and Nestin-Cre p75$^{in/in}$ brains were stained with the nuclear marker DAPI (Fig. 5A). Although the thickness of each layer in the knockout mice was significantly reduced compared with that in the control animals, the change was most pronounced in layers II/II and IV, which were reduced by 37.7±1.2% and 42.6±6.7%, respectively, whereas the deeper layers (V, VI) were less affected (Fig. 5B). When normalized to absolute cortical thickness, layers II/III and IV of Nestin-Cre p75$^{in/in}$ cortices remained reduced by 25.4±1.3% and 31.2±6.6%, respectively, compared with those of controls (Fig. 5C). No significant difference in the normalized thickness of layers I or VI was observed between genotypes, whereas the relative thickness of layer V of Nestin-Cre p75$^{in/in}$ mice was increased by 9.9±0.9% compared with that in control animals (Fig. 5C), potentially reflecting the increased apical dendritic complexity of pyramidal neurons residing in this layer.

To determine the pyramidal cell number in the upper and lower layers, histological sections of the somatosensory cortex were stained with the layer markers Tbr1 and Ctip2, respectively. Tbr1 identifies neurons in layers II/III and V/VI, while Ctip2 labels

Development (2019) 146, dev181933. doi:10.1242/dev.181933

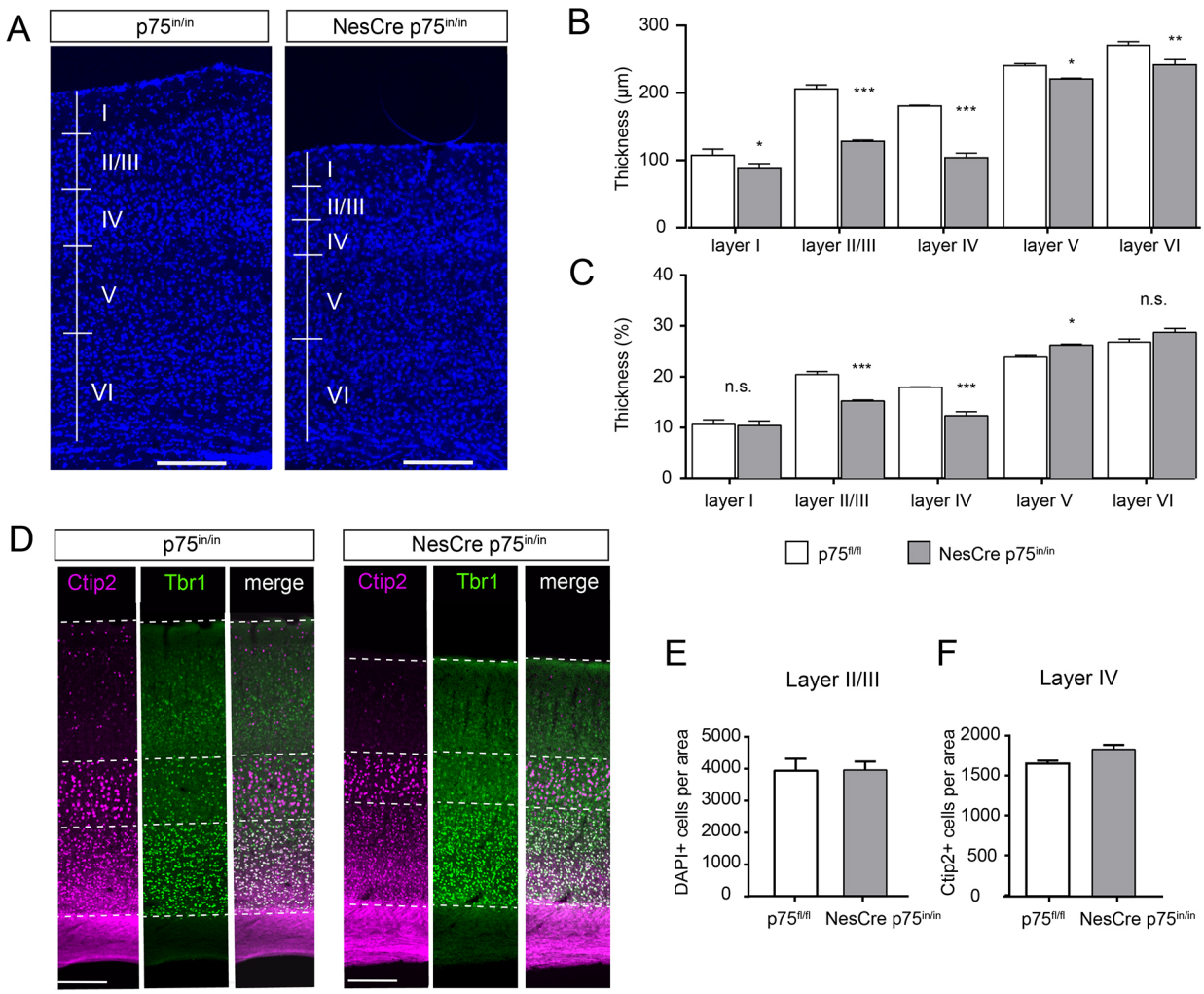

Fig. 5. Immunohistochemical analysis of cortical layering in Nestin-Cre (NesCre) p75$^{in/in}$ mice. (A) Image of DAPI-stained coronal sections of the somatosensory cortex of control (p75$^{fl/fl}$) and knockout (Nestin-Cre p75$^{in/in}$) mice at 3 months of age. Cellular density changes between layers were used to delineate layer boundaries. Scale bars: 400 µm. (B) Quantification of layer thickness (absolute) of the somatosensory cortex of control (p75$^{fl/fl}$) and knockout (Nestin-Cre p75$^{in/in}$) mice. Five matched sections per brain were measured. (C) Quantification of layer thickness normalized to whole cortical thickness. (D) Coronal sections of the brains of control (p75$^{fl/fl}$) and knockout (Nestin-Cre p75$^{in/in}$) mice immunostained for the cortical layer markers Ctip2 and Tbr1. Scale bars: 400 µm. (E,F) The cell densities in layer II/III (E) and layer IV (F) were measured by counting DAPI-positive nuclei (layer II/III) or Ctip2-positive cells (layer IV) and normalizing to area size. Cell counts were taken in five square areas per section in three sections per mouse. *n*=3 mice per genotype, data are mean±s.e.m., Student's *t*-test, **P*<0.05, ***P*<0.01, ****P*<0.001. n.s., not significant.

neurons residing in layers V/VI (Arlotta et al., 2005; Bulfone et al., 1995; Rubenstein et al., 1999). Apart from the obviously reduced upper layer thickness, the laminar architecture of pyramidal neuronal subtypes was grossly normal in the knockout mice (Fig. 5D). Furthermore, the density of DAPI-stained nuclei in layers II/III, as well as the number of nuclei and Ctip2-positive neurons in layer V were not significantly different (Fig. 5E,F). This indicates that the reduction in layer thickness is due to a decrease in absolute cell number. In particular, the number of later-born pyramidal cells within the upper cortical layers was more severely reduced by the developmental loss of p75^{NTR} than was the number of early-born deep layer pyramidal neurons.

We next analyzed the number of GABAergic interneurons, the second major neuronal type, in the cortex. Brain sections of adult control and Nestin-Cre p75$^{in/in}$ mice were stained for the interneuron markers parvalbumin, somatostatin, neuropeptide Y and calretinin (Fig. 6A). The number of interneurons of all subtypes analyzed were significantly reduced in the cortex of Nestin-Cre p75$^{in/in}$ mice compared with control mice (Fig. 6B). In particular, interneuron subtypes that are derived from the medial ganglionic eminence (MGE) and pre-optic area (POA) were found to be most severely affected, with a reduction of 50.1±4.8% for parvalbumin- and 44.1±3.0% for somatostatin-positive interneurons.

To assess whether other neurons derived from the MGE and POA (Anderson et al., 1997; Marin et al., 2000; Olsson et al., 1998; Zhao et al., 2003) were affected by the loss of p75^{NTR}, the number of cholinergic basal forebrain neurons, striatal cholinergic neurons and striatal parvalbumin-positive interneurons were counted (Fig. 6C,D). The absolute number of cholinergic basal forebrain neurons was significantly reduced (−32.7±9.5% compared with control), as was the number of striatal neurons (−64.0±3.6% and −26.7±3.8% for parvalbumin-positive neurons and cholinergic neurons, respectively) (Fig. 6E,F). However, when adjusted for the size of the respective brain areas, the number of cholinergic neurons was not changed in the basal forebrain compared with control, and the number of choline acetyltransferase (ChAT)-positive neurons in

Development (2019) 146, dev181933. doi:10.1242/dev.181933

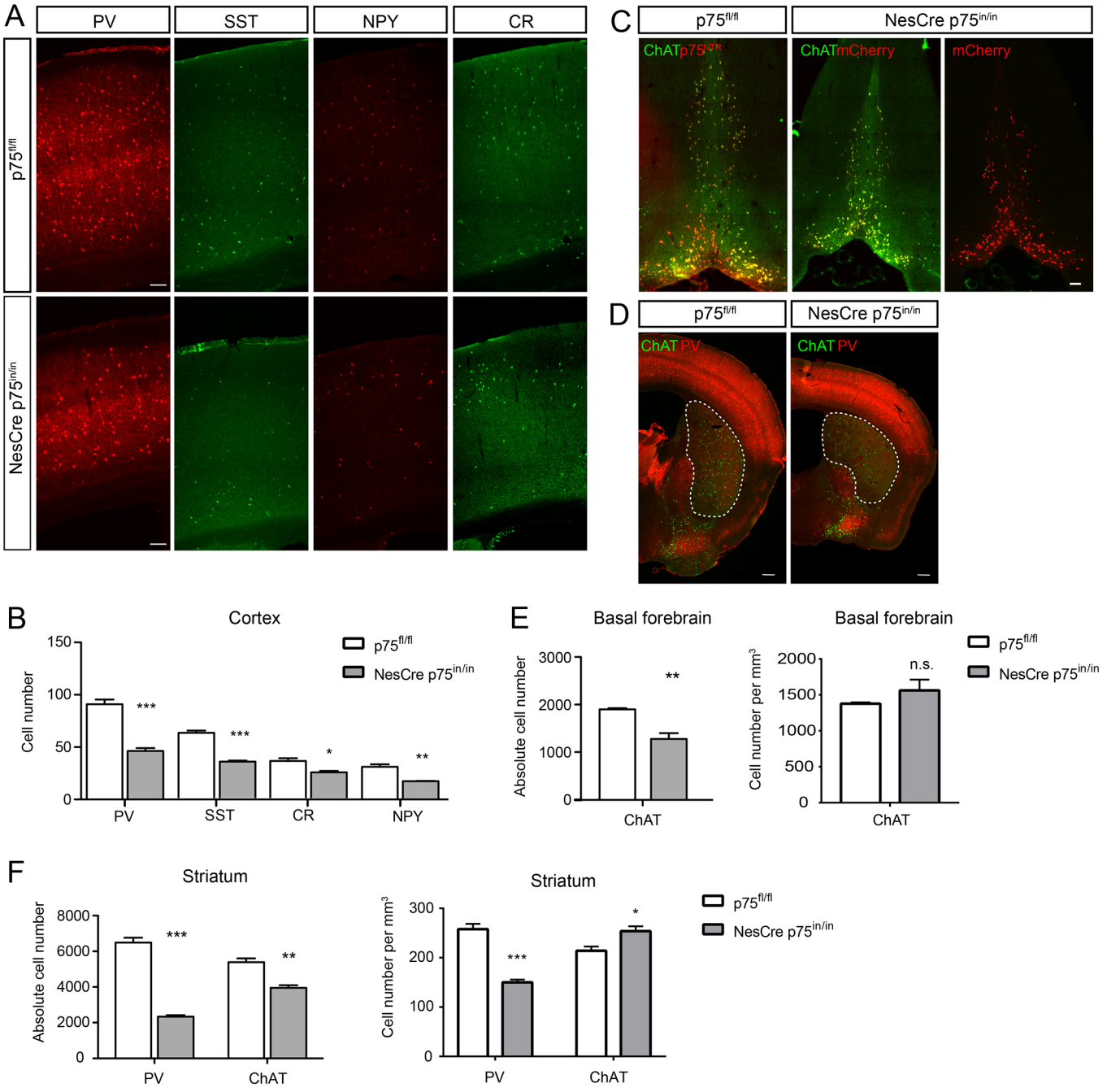

Fig. 6. Nestin-Cre (NesCre) p75$^{in/in}$ mice have reduced numbers of interneurons and cholinergic neurons. (A) Representative images of coronal brain sections of control (p75$^{fl/fl}$) and knockout (Nestin-Cre p75$^{in/in}$) mice immunostained for the interneuron markers parvalbumin (PV), somatostatin (SST), neuropeptide Y (NPY) and calretinin (CR) at P60. (B) Quantification of interneuron subtype numbers in the somatosensory cortex in a 400 µm wide region of interest spanning all layers. (C) Representative images of basal forebrain sections immunostained for choline acetyltransferase (ChAT) and p75^{NTR} (in control) or mCherry (in Nestin-Cre p75$^{in/in}$ mice). (D) Representative images of coronal sections at the level of the striatum of control (p75$^{fl/fl}$) and knockout (Nestin-Cre p75$^{in/in}$) mice immunostained for ChAT and PV. The striatum is outlined. (E) Quantification of the total number of cholinergic basal forebrain neurons (total cell count of every 3rd section) and absolute cell number normalized to the average basal forebrain volume of each strain measured by MRI. (F) Quantification of cholinergic neurons and PV-positive interneurons in the striatum (total cell count of every 3rd section), and cell number normalized to the average striatal volume of each strain measured by MRI. *n*=5 mice, data are mean±s.e.m., Student's *t*-test, **P*<0.05, ***P*<0.01, ****P*<0.001. n.s., not significant. Scale bars: 100 µm.

the striatum was proportionally increased in the knockout animals (+18.5±3.8%) (Fig. 6E,F). In contrast, the number of parvalbumin-positive interneurons in the striatum was proportionally decreased compared with the control. These findings demonstrate that the loss of p75^{NTR} in Nestin-expressing neural stem cells culminates in deficits to both dorsal and ventral telencephalic lineages, highlighting the crucial role of p75^{NTR} in cortical development.

p75^{NTR} is required for the survival of cortical neuron progenitors and production of later-born neurons

In order to investigate the cause of the reduced number of cortical neurons in the Nestin-Cre p75$^{in/in}$ mice, embryonic brains were collected at timepoints from E11.5 to E16.5, and sections were stained for the proliferation marker Ki67 and the apoptotic marker cleaved caspase 3. Whereas cleaved caspase 3-positive staining

Development (2019) 146, dev181933. doi:10.1242/dev.181933

was rarely seen in the p75$^{fl/fl}$ mice, the brains of embryonic Nestin-Cre p75$^{in/in}$ mice showed high numbers of apoptotic cells in all areas of the rostral telencephalon, particularly in the cortex, MGE and POA, consistent with the regions where p75^{NTR} expression is first detected (Fig. 1A; Fig. 7A-C). Increased numbers of apoptotic cells were first observed at E11.5, and were seen throughout the peak of neurogenesis, until ∼E16.5 (data not shown). Interestingly, although p75^{NTR} expression was primarily in post-mitotic neurons in wild-type mice, the apoptotic cells in Nestin-Cre p75$^{in/in}$ mice were situated in the proliferative zones that co-stained with the proliferation marker Ki67 (Fig. 7D-F), as well as in the intermediate zone of the cortex. Fewer dying neurons were observed in the cortical plate where p75^{NTR} expression is highest, suggesting that p75^{NTR} expression and function may begin prior to cell cycle exit, neuronal differentiation and/or migration into the cortical plate.

To explore this possibility, the progenitor-to-neuron ratio was assessed during early development in p75$^{fl/fl}$ and Nestin-Cre p75$^{in/in}$ mice. Dams were injected with BrdU 1 h prior to embryo collection to mark cells in the S-phase of mitosis. Neuronal lineage progression was then assessed in brain sections with immunostaining for BrdU and Ki67, or the cortical intermediate progenitor marker Tbr2 and neuronal marker Tbr1 (Englund et al., 2005; Fig. 8A,B). At E14.5, a significant reduction in proliferating S-phase progenitors was observed in Nestin-Cre p75$^{in/in}$ mice compared with controls (−16.9±2.8%; Fig. 8C). Similarly, a lower number of Tbr2-positive progenitors was observed in the knockout mice (−18.5±6.5%; Fig. 8D). In contrast, the number of Tbr1-positive neurons was not significantly reduced (Fig. 8E). Consistent with this result, at E12.5, the number of BrdU-positive cells that were Ki67 negative, i.e. had exited the cell cycle within the past 24 h (Kee et al., 2002), was unchanged in Nestin-Cre p75$^{in/in}$ mice compared with controls (Fig. 8F,G). However, in E14.5 embryos collected 24 h after BrdU administration, the number of newly produced neurons in Nestin-Cre p75$^{in/in}$ cortices was reduced by 41.4±4.9% compared with that in control brains, indicating that fewer later-born neuronal populations were being produced. This indicates that loss of p75^{NTR} affects the rate of neurogenesis in the second half of development. A similar reduction in the number of newborn neurons was also seen in the ganglionic eminences, as indicated by smaller size of the mantle zone (Fig. S5). This phenotype is consistent with the reduced number of cortical interneurons and later-born upper layer neurons of adult Nestin-Cre p75$^{in/in}$ mice.

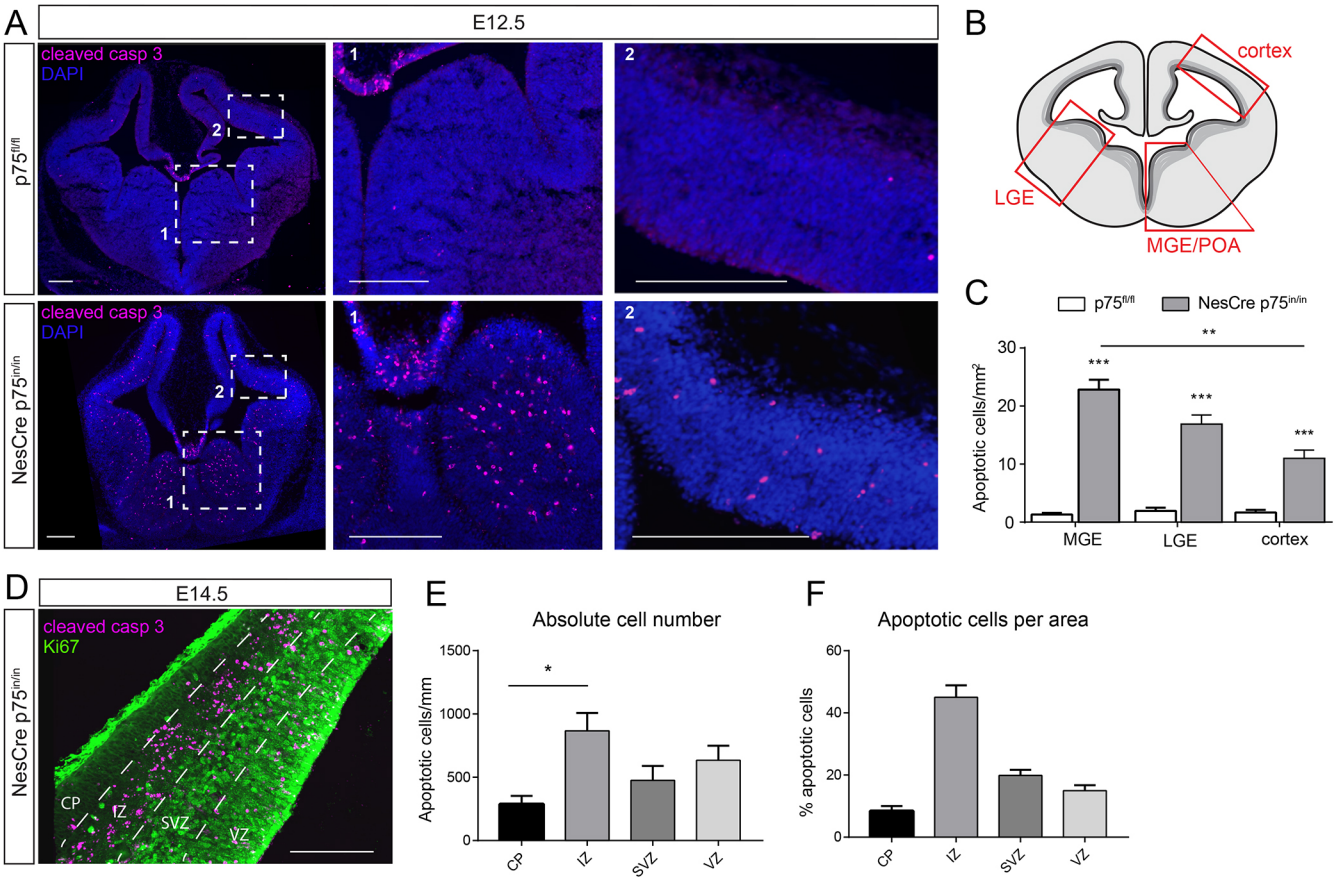

Fig. 7. Increased cleaved caspase 3 activation in the telencephalon of Nestin-Cre (NesCre) p75$^{in/in}$ mice. (A) Representative images of E12.5 control (p75$^{fl/fl}$) and knockout (Nestin-Cre p75$^{in/in}$) brain sections stained for cleaved caspase 3 and DAPI. Scale bars: 200 µm. The boxed regions illustrate cleaved caspase 3-positive cells in the medial ganglionic eminences (MGE) and neocortex. (B) Schematic representation indicating areas in which apoptotic cells were quantified. (C) Quantification of apoptotic (cleaved caspase 3 positive) cells in the cortex, MGE and lateral ganglionic eminences (LGE) in E12.5 control (p75$^{fl/fl}$) and knockout (Nestin-Cre p75$^{in/in}$) brain sections normalized to the total area. Student's *t*-test. (D) Image of E14.5 NesCre p75$^{in/in}$ cortical section stained for cleaved caspase 3 and Ki67, showing the distribution of apoptotic cells in the ventricular zone (VZ), subventricular zone (SVZ), intermediate zone (IZ) and cortical plate (CP). Scale bar: 150 µm. (E) Quantification of apoptotic (cleaved caspase 3 positive) cells per mm^2 in each zone. Two-way ANOVA followed by Tukey's post-hoc test. (F) Distribution of apoptotic cells across cortical areas as a percentage of total cleaved caspase 3-positive cells. *n*=3 mice, data are mean±s.e.m., **P*<0.05, ***P*<0.01, ****P*<0.001.

Development (2019) 146, dev181933. doi:10.1242/dev.181933

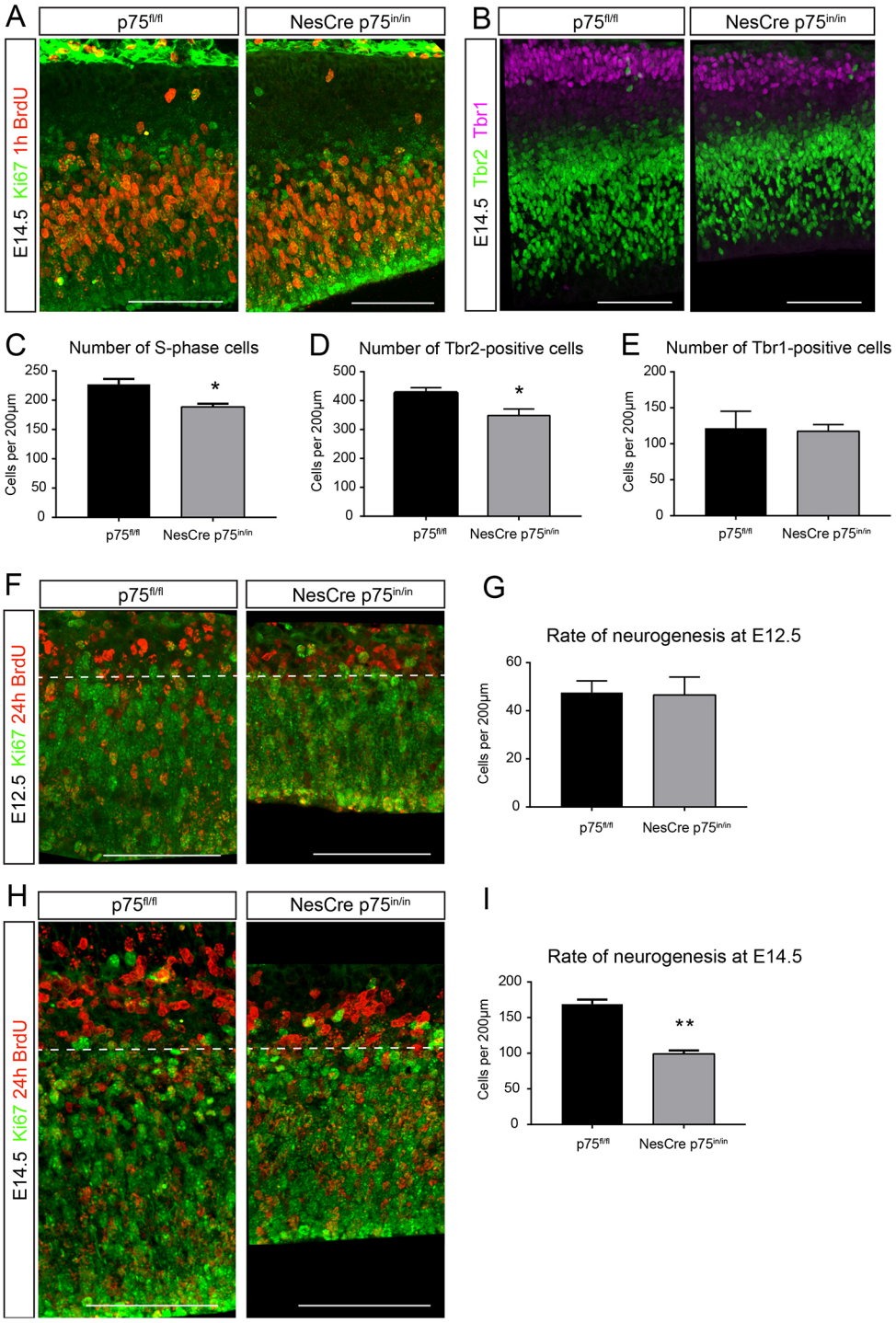

Fig. 8. Reduced number of proliferative cells and newborn neurons in Nestin-Cre (NesCre) p75$^{in/in}$ cortices.
(A) Representative images of E14.5 control (p75$^{fl/fl}$) and knockout (Nestin-Cre p75$^{in/in}$) cortical sections stained for BrdU and Ki67. BrdU was administered 1 h before embryo collection to label S-phase cells. (B) Representative images of E14.5 control (p75$^{fl/fl}$) and knockout (Nestin-Cre p75$^{in/in}$) cortical sections stained for the intermediate progenitor marker Tbr2 and neuronal marker Tbr1. (C) Quantification of S-phase (BrdU-positive) cells in the cortical sections of control and knockout mice at E14.5 in a 200 µm wide region of interest. *n*=3, Student's *t*-test. (D,E) Quantification of Tbr2-positive intermediate progenitor cells (D) and Tbr1-positive neurons (E) in cortical sections of control and knockout mice at E14.5 in a 200 µm wide region of interest. *n*=4, Student's *t*-test. (F) Representative images of E12.5 control (p75$^{fl/fl}$) and knockout (Nestin-Cre p75$^{in/in}$) cortical sections stained for BrdU and Ki67. BrdU was administered 24 h before embryo collection to label newborn neurons. (G) Quantification of post-mitotic (BrdU-positive, Ki67-negative) cells at E12.5 in a 200 µm wide region of interest. *n*=3, Student's *t*-test. (H) Representative images of E14.5 control (p75$^{fl/fl}$) and knockout (Nestin-Cre p75$^{in/in}$) cortical sections stained for BrdU and Ki67. BrdU was administered 24 h before embryo collection to label newborn neurons. (I) Quantification of post-mitotic (BrdU-positive, Ki67-negative) cells at E14.5 in a 200 µm wide region of interest. *n*=3 mice, data are mean ±s.e.m., Student's *t*-test, **P*<0.05, ***P*<0.01. Scale bars: 100 µm.

DISCUSSION

In this study, we assessed the role of p75^{NTR} in brain development. We first mapped the spatiotemporal expression of p75^{NTR} in the developing mouse telencephalon. We found that expression begins around E11.5 in the rostroventral part of the brain, while expression in the cortex starts ∼1 day later and continues until postnatal stages. p75^{NTR} immunostaining mainly colocalized with the neuronal marker βIII tubulin and was strongest outside the proliferative zones, suggesting that p75^{NTR} is expressed by post-mitotic cells rather than neuronal progenitors. However, in previous studies, p75^{NTR} mRNA was found in progenitors of the ventricular and subventricular zones, as well as in the areas where post-mitotic cells reside (Kendall et al., 2002). Therefore, transcription may precede p75^{NTR} protein expression, or translation may be below the detection threshold of immunostaining in progenitor cells. Indeed, it has been shown that p75^{NTR} can regulate the cell cycle and facilitate the cell cycle exit of neuronal cells (Vilar et al., 2006; Zanin et al., 2016; Zhang et al., 2009). p75^{NTR} also affects the cell cycle in cancer cells of a range of tissue types, including glioma metastases, prostate cancer cells and breast cancers (Johnston et al., 2007; Krygier and Djakiew, 2002; Verbeke et al., 2010). It is therefore plausible that p75^{NTR} upregulation occurs and is required

Development (2019) 146, dev181933. doi:10.1242/dev.181933

for neurogenic divisions and/or the timely cell cycle exit of telencephalic progenitors.

To investigate the neurodevelopmental function of $p75^{NTR}$, we crossed a $p75^{NTR}$ floxed strain to a line expressing Cre-recombinase under the control of the nestin promoter (Nestin-Cre), creating a mouse strain in which deletion of the $p75^{NTR}$ gene is specific to neuronal progenitors. Nestin expression starts around E10 in mice, and therefore $p75^{NTR}$ expression is lost shortly before the onset of neurogenesis (Dubois et al., 2006). The most obvious phenotype observed in adult Nestin-Cre $p75^{in/in}$ mice was their reduced size. A similar decrease has been reported upon deletion of $p75^{NTR}$ exon IV (von Schack et al., 2001), but not in $p75^{NTR}$ exon III-deficient mice (Lee et al., 1994). However the latter mice can retain expression of a functional truncated version of $p75^{NTR}$, which may account for the discrepancy in these observations (Boskovic et al., 2014; von Schack et al., 2001). Although Nestin is predominantly expressed in the progenitors of the developing brain, there is evidence for its expression in other tissues, including developing cardiomyocytes, presomitic mesoderm, myotome and dermatone, and endothelial cells of developing blood vessels (Wiese et al., 2004). It is therefore conceivable that a secondary effect of $p75^{NTR}$ knockout in other non-neuronal tissues, such as defects in the vascular system, may have contributed to the reduced body size of the Nestin-Cre $p75^{in/in}$ mice. Alternatively, the parental Nestin-Cre strain has been reported to have reduced body size, which is thought to be the result of mild hypopituitarism (Declercq et al., 2015). Although this phenotype was not apparent in our parental strain or Nestin-Cre $p75^{WT/in}$ heterozygous mice (Fig. S1D), it is possible that the reduced body size is unrelated to the loss of $p75^{NTR}$, and the overall smaller brain in the mutant mice was an indirect effect. To correct for this possibility, the relative change in brain region sizes was assessed by normalizing the data to the whole brain, revealing disproportionate reduction in the volume of the cortex and basal ganglia, correlating with reduced numbers of cortical pyramidal neurons, interneurons, and striatal and basal forebrain neurons. Furthermore, a fissure was observed along the thalamus that was not present in the control mice. This appears to be caused by impaired midline fusion during early postnatal development, which prevents the contralateral migration of thalamic neurons. The multitude of phenotypes observed in the Nestin-Cre $p75^{in/in}$ mice likely reflects different roles that $p75^{NTR}$ plays in the development of these structures and indicates that its expression is required for their adequate formation. As the neocortex was one of the structures that was most severely affected by the embryonic loss of $p75^{NTR}$, and a specific role for $p75^{NTR}$ in the development of this area has not been described, we focused our study on the changes that occurred during early cortical development.

The neocortex of adult Nestin-Cre $p75^{in/in}$ mice contained significantly fewer later-born, upper layer neurons than control mice, but equivalent numbers of early born pyramidal neurons when normalized to total cortical thickness. Cortical layers are formed in an inside-out fashion during development, creating the deep layer neurons first, followed by the upper layers (Gilmore and Herrup, 1997). A reduction in upper layer size therefore reflects a defect in later-born neurons rather than early born populations. However, deeper layer pyramidal neurons displayed increased apical dendritic complexity. Increased dendritic complexity has previously been reported for hippocampal neurons lacking $p75^{NTR}$ (Zagrebelsky et al., 2005), and this phenotype could therefore be due to an intrinsic lack of $p75^{NTR}$ in these cells, although other non-cell-autonomous effects, such as reduced inhibitory control or compensation for the reduced number of upper layer pyramidal neurons, are also possible explanations for the dendritic complexity phenotype.

The reduction of neuronal number in Nestin-Cre $p75^{in/in}$ mice can be explained, at least partially, by the observed apoptosis of telencephalic progenitors during early stages of neurogenesis. Increased cell death was detected throughout the developing Nestin-Cre $p75^{in/in}$ brain at E12.5, with the most obvious increase in apoptotic cells found in the ventral part of the telencephalon, notably in the MGE and POA. The ganglionic eminences are transient structures that have been identified as the birthplace of interneurons (Anderson et al., 1997), and the MGE also gives rise to basal forebrain neurons (Zhao et al., 2003). When normalized to the volume of the respective brain areas, the number of cholinergic cells was unchanged in the basal forebrain, whereas in the striatum it was proportionally increased in the knockout animals. It has previously been shown that a conditional knockout of $p75^{NTR}$ in a ChAT-Cre $p75^{in/in}$ mouse strain leads to an increase in the number of cholinergic neurons in the basal forebrain due to inhibition of naturally occurring cell death (Boskovic et al., 2014). Therefore, the loss of progenitors of cholinergic neurons might be partially compensated during postnatal development. In contrast, the number of parvalbumin-positive interneurons in the striatum was proportionally decreased compared with the control, suggesting that the loss of interneuron progenitors cannot be compensated for by a similar mechanism. Thus, the significant reduction in interneuron number in the striatum and in all layers of the cortex in adult Nestin-Cre $p75^{in/in}$ mice can be attributed to the extensive apoptosis of ventral progenitors.

Similarly, an increased number of apoptotic cells was also evident in the proliferative zones of the developing cortex, coincidental with a decreased number of S-phase cells and Tbr2-positive intermediate progenitors at E14.5. In contrast, apoptosis was rarely observed in the cortical plate where mature neurons reside, and the number of Tbr1-positive neurons did not change significantly. Nonetheless, a marked decrease in the production of mature neurons was apparent during the peak of neurogenesis at E14.5, when neurons destined for the late-born upper cortical layers are being produced.

During the early stages of cortical neurogenesis, neurons are principally created from highly proliferative radial glial progenitors located in the ventricular zone, which can produce one immature neuron and one identical daughter cell by asymmetric division. Later, these progenitors switch to a two-stage process, producing intermediate progenitor cells, which, after a few rounds of proliferative divisions in the subventricular zone, undergo neurogenic divisions to produce two neurons (Chen et al., 2015; Englund et al., 2005; Pontious et al., 2008). Therefore, in Nestin-Cre $p75^{in/in}$ mice, a change in the fate of dividing radial glial progenitors could either lead to depletion of the stem cell pool through a reduction of self-renewing divisions or result in the production of fewer intermediate progenitor cells, both of which would result in fewer later-born neurons being generated. An alternative explanation is that while the production of neurons and intermediate progenitor cells from radial glial cells is normal, the intermediate progenitor cells have reduced capacity for division or differentiation. The last idea is more consistent with our observations, as the majority of apoptotic cells were found in the subventricular zone and intermediate zone rather than the ventricular zone, with more dying cells in the cortex at E14.5 than E12.5, indicative of an intermediate progenitor cell phenotype. Death of the intermediate progenitor cells during failed division or differentiation, resulting in reduced production of late-born cortical

Development (2019) 146, dev181933. doi:10.1242/dev.181933

neurons, provides a parsimonious explanation for the disproportionate reduction in upper layer neurons in adult Nestin-Cre p75$^{in/in}$ mice. p75^{NTR} upregulation in intermediate progenitor cells prior to, or immediately after, their final neurogenic division is therefore important for normal cortical neurogenesis.

However, other non-cell-autonomous effects of p75^{NTR} may have also contributed to the reduction in cortical neuronal number in Nestin-Cre p75$^{in/in}$ mice. The reduced number of S-phase cells in the cortex could indicate that the cell cycle length of progenitor cells is affected, as has been reported for other neural populations (Vilar et al., 2006; Zanin et al., 2016; Zhang et al., 2009). Furthermore, it has recently been reported that the proliferation of pyramidal neuron progenitors is controlled by the rate of cortical invasion of migrating interneurons, with higher levels of proliferation observed if more interneurons invade at the same time (Silva et al., 2018). Similarly, a mouse strain harboring a deletion of the transcription factor Nkx2.1, a master regulator of interneuron development, showed attenuated proliferation of pyramidal neuron progenitors, consistent with the idea that the number of pyramidal neurons is fine-tuned and adjusted during development according to the number of invading interneurons, thereby ensuring the proper formation of local networks (Butt et al., 2008; Silva et al., 2018). Therefore, the phenotype observed in Nestin-Cre p75$^{in/in}$ mice may reflect a combination of cell-autonomous and non-cell-autonomous effects, resulting in the impaired survival and proliferative capacity of cortical progenitors. It remains to be determined to what extent each of these factors contributes to the phenotype.

The multitude of signaling cascades that are controlled by p75^{NTR}, and the highly context-specific outcome of p75^{NTR} activation, underpin the need for targeted conditional knockout mouse models. Interestingly, the severe apoptotic phenotype observed in Nestin-Cre p75$^{in/in}$ mice is not observed in mice harboring a complete knockout of the p75^{NTR} gene (Fig. S6). p75^{NTR} is expressed in embryonic stem cells (Moscatelli et al., 2009), and is absent from the moment of fertilization in complete knockout mice, whereas Nestin-Cre p75$^{in/in}$ mice develop normally until gene deletion is initiated in neural progenitors around E10. Developmental programs have been shown to have high levels of redundancy that are thought to ensure robustness. It is therefore likely that cells in complete p75^{NTR} knockout mice rely on alternative mechanisms that ensure appropriate early embryonic development and that continue to be used in neural progenitor populations. Initiation of compensatory mechanisms or alternative signaling routes may not be possible after a certain degree of specification has been reached, leaving progenitors in Nestin-Cre p75$^{in/in}$ mice vulnerable to the loss of p75^{NTR}.

In summary, we have found that conditional knockout of the p75^{NTR} gene in neuronal progenitors in Nestin-Cre p75$^{in/in}$ mice results in structural abnormalities of the brain, including a marked decrease in brain volume and impaired thalamic midline closure. However, p75^{NTR} deficiency did not affect all brain areas to the same extent; when normalized to the whole-brain volume, the basal forebrain and neocortex were most significantly reduced. The numbers of adult and developing cortical projection neurons and interneurons were decreased, consistent with increased apoptosis of progenitors of these cells in the embryo and with the reduced rates of neurogenesis, which likely accounts for the total reduction in cortical volume. Given that these two major classes of cortical neurons originate from spatially and transcriptionally distinct progenitor zones, these results suggest that p75^{NTR} fulfils a generic role in the production, differentiation and/or survival of these neuronal progenitors.

MATERIALS AND METHODS

Mice

All procedures were approved by the University of Queensland Animal Ethics Committee and conducted in accordance with the Australian Code of Practice for the Care and Use of Animals for Scientific Purposes. The p75^{NTR} floxed and the Nestin-Cre transgenic knock-in mouse strains have been described previously (Boskovic et al., 2014; Tronche et al., 1999). Briefly, the p75^{NTR} floxed strain harbors a transgenic construct containing a floxed exon 1 of *p75^{NTR}* (*NGFR*/*TNF16*) as well as an inverted *mCherry* reporter gene and stop codon. Upon Cre expression, the construct is inverted and p75^{NTR} expression switched for mCherry (p75$^{in/in}$). Both male and female animals were used for all experiments (2-6 months old). Genotyping was performed by The University of Queensland Australian Equine Genetics Research Centre (AEGRC).

Tissue preparation

The day of vaginal plug detection was considered E0.5 and birth was considered as postnatal day 0 (P0). For embryos younger than E16.5, whole-embryo heads were drop-fixed overnight in 4% paraformaldehyde (PFA) in phosphate-buffered saline (PBS) before processing for histological analysis. The brains of E14.5 and older embryos were dissected from the skull after drop fixation. E16.5 embryos were transcardially perfused with 4% PFA, after which whole heads were post-fixed overnight, and the brains dissected from the skull. Adult mice were deeply anesthetized with sodium pentobarbitone (VIRBAC) and perfused with 4% PFA through the left ventricle of the heart. Brains were removed from surrounding tissues and post-fixed in 4% PFA. Unless stated otherwise, fixed samples were cryo-protected overnight by immersion in 20% sucrose/PBS before cryosectioning. Embryonic coronal tissue sections (30 µm) were collected on Superfrost Plus slides. Staining of adult tissues (P60 and older) was performed on 40 µm coronal sections.

BrdU injections

5-Bromo-2′-deoxyuridine (BrdU, Sigma) was dissolved in PBS with 1% dimethyl sulfoxide (DMSO). Pregnant dams were injected intraperitoneally either 1 h or 24 h before embryo collection with 50 mg/kg BrdU solution.

Nissl staining

Floating sections (40 µm) were mounted on Superfrost Plus slides and allowed to dry, dehydrated in 100% ethanol, after which they were defatted for 15 min in xylene. The sections were rehydrated in 95% and 70% ethanol and H_2O, then stained in 0.1% Cresyl Violet acetate solution for 10 min. The stained sections were rinsed in H_2O and destained with 70% ethanol until the desired intensity was reached, at which point the reaction was stopped by immersing slides into 100% ethanol followed by xylene. The sections were then mounted in DePex mounting medium (VWR International).

Immunolabeling

For immunofluorescence labeling without antigen retrieval, tissue sections were incubated for 1 h in blocking buffer (5% horse serum, 0.1% Triton-X 100 in PBS). The sections were then incubated overnight at room temperature in primary antibody diluted in blocking buffer. They were subsequently washed in PBS containing 0.1% Triton-X 100 at room temperature before being incubated with the appropriate fluorescent secondary antibody (1/1000; Jackson Immunoresearch Laboratories) for 2 h at room temperature and protected from light. Cell nuclei were stained with DAPI (1/2000, Sigma). Sections were mounted on Superfrost slides and coverslipped with Dako mounting medium.

For immunofluorescence labeling with antigen retrieval, tissue sections were mounted onto Superfrost slides and allowed to dry completely before incubating in 10 µM sodium citrate buffer at 85°C for 30 min. The slides were then washed in PBS and the subsequent blocking, antibody incubation and mounting steps were performed as described above.

Bright-field immunohistochemistry was performed as described previously (Hamlin et al., 2013). Briefly, sections were washed in 0.1 M phosphate buffer (PB, pH 7.4), and then incubated in 3% H_2O_2 and 50% ethanol to inactivate endogenous peroxidase. The sections were

Development (2019) 146, dev181933. doi:10.1242/dev.181933

subsequently washed in 0.1 M PB, and incubated for 1 h at room temperature in blocking solution (PB, 10% horse serum and 0.1% Triton-X 100). Primary antibodies were diluted in blocking buffer before being applied onto the sections for overnight incubation at room temperature. The sections were then washed at room temperature in PBS containing 0.1% Triton-X 100 before incubation with biotinylated secondary antibody and ABC reagents (Vector Elite Kit, Vector Laboratories; 6 µl/ml avidin and 6 µl/ml biotin). Black immunoreactivity was revealed by a nickel-intensified diaminobenzidine reaction. Sections were then washed in PB and gradually dehydrated in ethanol and xylene before being mounted in DePex mounting medium (VWR International).

Primary antibodies

Primary antibodies included goat anti-$p75^{NTR}$ (extracellular domain; immunofluorescence 1/200; immunohistochemistry 1/1000; R&D Systems, AF1157), rabbit anti-Ds Red (1/500; Clontech, 632496), mouse anti-parvalbumin (1/1000; Millipore, MAB1572), rabbit anti-calretinin (1/2000; Swant, 7699/3H), rabbit anti-activated caspase 3 (1/500; Cell Signaling, 9661L) and mouse anti-β3 tubulin (TUJ1; 1/2000; Promega, G712A), used without antigen retrieval (for embryonic tissue, the anti-$p75^{NTR}$ antibody was found to work best on vibratome sections using non-frozen tissue). In addition, rat anti-Ctip2 (1/500; Abcam, ab18465), rabbit anti-Tbr1 (1/500; Abcam, ab31940), rat anti-EOMES (Tbr2) (1/500; Life Technologies, 53-4875-80), rat anti-somatostatin (1/1000; Millipore, MAB354), rabbit anti-neuropeptide Y (NPY) (1/2000; Immunostar, 22940), mouse anti-Ki67 (1/500; BD Biosciences, 556003) and rat anti-BrdU (1/500; Serotec, MCA2060) were used following antibody retrieval.

Golgi-Cox staining

Mice were perfused transcardially with 0.04% PFA in NaCl, and their brains were removed. The brains were incubated in Golgi-Cox solution overnight, with the Golgi-Cox solution being replaced the next day, and again after 1 week. After 2 weeks, the brains were placed in 30% sucrose in NaCl for 3 days and subsequently sectioned into 150 µm slices using a vibratome. Tissue sections were mounted onto gelatin-coated Superfrost Plus slides and dried at 4°C for 24 h, followed by another 24 h at room temperature. To visualize the staining, sections were washed sequentially in distilled H_2O for 1 min, in 30% ammonia for 10 min and in fresh ammonia (30%) for 10 min. Following a distilled H_2O wash, the sections were incubated for 5 min in 5% thiosulphate, followed by another 5 min in fresh thiosulphate (5%), before being washed for 3 min in each of 30% and 70% ethanol, twice for 5 min in 100% ethanol and >1 h in xylene.

Quantification

For quantification of immunohistochemical staining, a minimum of three mice were used for each genotype. To ensure that the same cutting angle was applied between experimental groups, embryonic coronal sections were matched using four points of reference: choroid plexus/cortical hem and preoptic area/medial ganglionic eminences for dorsal and ventral, and the lateral ganglionic eminences for lateral orientation. Cell counts, cell size, and volume and thickness measurements of the cortex and striatum were performed using Imaris 7.2.3 software (Bitplane) and ImageJ. Quantification of the number of cortical interneurons in the adult brain was performed in a defined area of the cortex (400 µm width, 40 µm depth) spanning the pial-white matter extent of the cortex. Cell density was calculated as the number of cells in regions of interest of equal size that covered layers V and VI. Neurolucida Neuron Tracing Software (MBF Bioscience) was used to measure neurite length and soma size in Golgi-Cox samples, and to perform Sholl and complexity analyses. Neurite complexity was calculated as described previously (Pillai et al., 2012). Neurons were selected for tracing according to their location (layer V in the somatosensory cortex), position in the section (soma roughly in the center, no dendrites cut off) and minimal overlap with other neurons.

BDA injections

Two-day-old animals were anesthetized by placing them on ice and keeping them cool throughout the procedure. Each mouse was placed in a stereotaxic frame (David Kopf Instruments) and the skull was maintained in a flat position. Unilateral infusion of biotinylated dextran-amide (BDA, 10,000 MW, Invitrogen) was performed using a glass needle. The needle was lowered into the thalamus, and infusions were conducted over 2 min (0.5 µl); the needle was then left in place for 2 min to allow for diffusion. Immediately after surgery, the mice were allowed to recover by placing them on a warm surface before they were returned to their cage. Mice were sacrificed by perfusion 3 days after the procedure.

Magnetic resonance imaging

Three-month-old mice were perfused transcardially with 4% PFA as described above and whole heads were post-fixed overnight. Brains were removed from the skull the next day and immersed in 0.1 M PBS with 0.2% gadopentetate dimeglumine (Magnevist, Bayer) for 4 days. A small animal magnetic resonance imaging (MRI) system (16.4T vertical bore; Bruker Biospin; ParaVision v6.01) with a 15 mm linear SAW coil (M2M Imaging) and a Micro2.5 imaging gradient was used. Three-dimensional (3D) diffusion-weighted imaging spin-echo sequences were acquired with the following parameters: echo time (TE)=23 ms, repetition time (TR)=200 ms, signal average (NA)=1, diffusion pulse/mixing times (δ/Δ)=2.5/12 ms, spectral bandwidth=50 kHz, 30 direction diffusion-encoding with b-value=5000 s/mm^2, 2 b=0 images (without diffusion-weighting) and a field of view (FOV)=19.6×11.4×8.4 mm with matrix=196×114×84 to produce images at 0.1 mm isotropic resolution. The acquisition time was 17 h. A 3D gradient echo Fast Low Angle Shot (FLASH) sequence was acquired with TR/TE=50/12 ms, 30° flip angle, NA=1, the same spectral bandwidth and FOV as the DWI sequence but with matrix=654×380×280 to produce images at 0.03 mm isotropic resolution; the acquisition time was 40 min.

Volumetric analysis was performed using an adult C57/BL6 MRI brain atlas developed in-house at the Centre for Advanced Imaging (CAI) at the University of Queensland (Liu et al., 2016; Ullmann et al., 2014), and the Brookhaven C57/BL6 *ex vivo* brain MRI atlas (Ma et al., 2005). These atlases were registered into the FLASH images using FMRIB Software Library linear and non-linear registration (FLIRT and FNIRT) (Jenkinson et al., 2012). Measurements were extracted using ITK-SNAP (www.itksnap.org; Yushkevich et al., 2006). The volume of the basal forebrain was measured by drawing a region of interest on the diffusion-weighted fractional anisotropy (FA) image using the mouse brain atlas by Paxinos and Franklin (2007) as a guide and as described previously (Kerbler et al., 2013).

Statistical analysis

Graphs were created using GraphPad Prism version 7.0. Unless stated otherwise, results are displayed as mean±s.e.m. Statistical testing was performed using a Student's *t*-test, one- or two-way ANOVA, or Chi-squared test.

In situ hybridization

All solutions used for *in situ* hybridization were pre-treated with 0.1% DEPC. Cryostat sections (14 µm) of E12.5 embryonic brains were collected onto Superfrost Plus microscope slides (VWR International). Hybridization buffer containing the antisense RNA probe was applied to the slides and covered with a coverslip. The slides were then incubated overnight at 65°C in a humid chamber [50% formamide; 1× saline-sodium citrate (SSC)]. The hybridization buffer contained 50% deionized formamide (Sigma), 2 M NaCl, 50 mM EDTA, 100 mM Tris-HCl (pH 7.5), 50 mM NaH_2PO_4, 50 mM Na_2HPO_4, 0.1 mg/ml tRNA from bakers' yeast (Roche Diagnostics), 1× Denhardt's solution (Sigma) and 10% dextran sulphate. After hybridization, sections were washed three times for 30 min in wash solution (50% formamide, 1× SSC, 0.1% Tween 20) at 65°C and twice in 1× MABT [100 mM maleic acid, 150 mM NaCl (pH 7.5), 0.1% Tween 20] at room temperature. They were then blocked in 2% Blocking Reagent (Roche Diagnostics) and 10% heat-inactivated goat serum (Sigma) in 1× MABT for 1 h at room temperature followed by overnight incubation at 4°C in anti-DIG antibody conjugated to alkaline phosphatase (Roche Diagnostics) diluted at 1/1500 in blocking solution. The sections were then washed three times for 15 min in 1× MABT at room temperature before being incubated for 15 min in equilibration buffer [100 mM NaCl, 100 mM Tris-HCl (pH 9.5), 0.1% Tween 20]. Staining was developed at 37°C for 4 to 8 h in staining solution containing 100 mM NaCl, 50 mM $MgCl_2$, 100 mM Tris-HCl (pH 9.5),

0.1% Tween 20, nitroblue tetrazolium (4.5 µl/ml; Roche Diagnostics), 5-bromo-4-chloro-3-indolyl phosphate (3.5 µl/ml; Roche Diagnostics) and 5% polyvinylalcohol. Finally, the sections were washed in distilled water and gradually dehydrated in ethanol and xylene before being mounted in DePex mounting medium (VWR International) (Delogu et al., 2012).

Behavioral testing

Male and female six-month-old *Nestin-Cre* $p75^{in/in}$ and $p75^{fl/fl}$ mice were used for all behavioral tests. Animals were maintained on a 12 h light/dark cycle (lights on at 7:00 a.m.), with food and water provided *ad libitum*. Animals were adjusted to the experimental facilities for at least 30 min before commencement of behavioral tests.

Rotarod and grip strength motor function testing

The mice were placed on a rotating rod and the time until they fell off was measured. The initial rotarod speed was set to 4 rpm and was gradually increased (acceleration rate of 1 rpm/s) until a maximum speed of 40 rpm. The mice were left on the rotating bar for a maximum of 120 s. Fore- and hind-limb grip strength was tested by pulling mice evenly across a metal bar attached to a grip strength meter (Harvard apparatus). Three measurements were taken per animal and limb pair then averaged.

Elevated plus maze

Each mouse was placed in an elevated plus maze apparatus (Pellow et al., 1985) for 5 min under bright light conditions (400 lux) with the total time spent in the open and closed arms being measured using EthoVision XT tracking software (Noldus).

Novel arm recognition test

Mice were placed in a Y maze with one arm of the maze closed off (left and right were alternated randomly between animals) for 10 min, as described previously (Qian et al., 2018). Novel arm recognition was tested 24 h after training by placing the mice back into the Y maze with all arms open for 5 min at 150 lux, and time spent in each arm was measured using the EthoVision XT tracking software (Noldus).

Acknowledgements

We acknowledge the support of the Queensland NMR Network and the National Imaging Facility (a National Collaborative Research Infrastructure Strategy capability) for the operation of a 16.4T MRI at the Centre for Advanced Imaging, the University of Queensland. Optical imaging using wide-field fluorescence microscopes and slide scanners, and image analysis using Neurolucida were performed at the Queensland Brain Institute's Advanced Microscopy Facility, generously funded through ARC LIEF grant LE130100074. We thank the staff of the University of Queensland Biological Resources Facility for breeding and maintaining the animals used in this study, members of the Coulson laboratory past and present for helpful discussions and Rowan Tweedale for editorial assistance.

Competing interests

The authors declare no competing or financial interests.

Author contributions

Conceptualization: S.M., F.A., M.P., E.J.C.; Methodology: S.M., F.A., N.D.K., E.J.C.; Software: N.D.K.; Validation: S.M., F.A.; Formal analysis: S.M., F.A., N.D.K.; Investigation: S.M., F.A., N.D.K., M.R.M., M.A.K., A.D.; Resources: M.P., E.J.C.; Data curation: S.M., F.A., N.D.K.; Writing - original draft: S.M., F.A.; Writing - review & editing: S.M., M.P., E.J.C.; Visualization: S.M., F.A., E.J.C.; Supervision: M.P., E.J.C.; Project administration: S.M., F.A., E.J.C.; Funding acquisition: E.J.C.

Funding

S.M. is supported by an International Postgraduate Research Scholarship, a University of Queensland Centennial Scholarship and a Queensland Brain Institute Top-up scholarship. E.J.C. receives support from the Clem Jones Centre for Ageing Dementia Research and the Australian Research Council (ARC LP110100403).

Supplementary information

Supplementary information available online at
http://dev.biologists.org/lookup/doi/10.1242/dev.181933.supplemental

References

Anderson, S. A., Eisenstat, D. D., Shi, L. and Rubenstein, J. L. (1997). Interneuron migration from basal forebrain to neocortex: dependence on Dlx genes. *Science* **278**, 474-476. doi:10.1126/science.278.5337.474

Andrews, G. L., Yun, K., Rubenstein, J. L. R. and Mastick, G. S. (2003). Dlx transcription factors regulate differentiation of dopaminergic neurons of the ventral thalamus. *Mol. Cell. Neurosci.* **23**, 107-120. doi:10.1016/S1044-7431(03)00016-2

Arlotta, P., Molyneaux, B. J., Chen, J., Inoue, J., Kominami, R. and Macklis, J. D. (2005). Neuronal subtype-specific genes that control corticospinal motor neuron development in vivo. *Neuron* **45**, 207-221. doi:10.1016/j.neuron.2004.12.036

Bernabeu, R. O. and Longo, F. M. (2010). The p75 neurotrophin receptor is expressed by adult mouse dentate progenitor cells and regulates neuronal and non-neuronal cell genesis. *BMC Neurosci.* **11**, 136. doi:10.1186/1471-2202-11-136

Boskovic, Z., Alfonsi, F., Rumballe, B. A., Fonseka, S., Windels, F. and Coulson, E. J. (2014). The role of p75NTR in cholinergic basal forebrain structure and function. *J. Neurosci.* **34**, 13033-13038. doi:10.1523/JNEUROSCI.2364-14.2014

Bulfone, A., Smiga, S. M., Shimamura, K., Peterson, A., Puelles, L. and Rubenstein, J. L. R. (1995). T-brain-1: a homolog of Brachyury whose expression defines molecularly distinct domains within the cerebral cortex. *Neuron* **15**, 63-78. doi:10.1016/0896-6273(95)90065-9

Butt, S. J. B., Sousa, V. H., Fuccillo, M. V., Hjerling-Leffler, J., Miyoshi, G., Kimura, S. and Fishell, G. (2008). The requirement of Nkx2-1 in the temporal specification of cortical interneuron subtypes. *Neuron* **59**, 722-732. doi:10.1016/j.neuron.2008.07.031

Cattaneo, E. and McKay, R. (1990). Proliferation and differentiation of neuronal stem cells regulated by nerve growth factor. *Nature* **347**, 762-765. doi:10.1038/347762a0

Catts, V. S., Al-Menhali, N., Burne, T. H. J., Colditz, M. J. and Coulson, E. J. (2008). The p75 neurotrophin receptor regulates hippocampal neurogenesis and related behaviours. *Eur. J. Neurosci.* **28**, 883-892. doi:10.1111/j.1460-9568.2008.06390.x

Chen, C., Lee, G. A., Pourmorady, A., Sock, E. and Donoghue, M. J. (2015). Orchestration of neuronal differentiation and progenitor pool expansion in the developing cortex by SoxC genes. *J. Neurosci.* **35**, 10629-10642. doi:10.1523/JNEUROSCI.1663-15.2015

Chittka, A. and Chao, M. V. (1999). Identification of a zinc finger protein whose subcellular distribution is regulated by serum and nerve growth factor. *Proc. Natl. Acad. Sci. USA* **96**, 10705-10710. doi:10.1073/pnas.96.19.10705

Colditz, M. J., Catts, V. S., Al-menhali, N., Osborne, G. W., Bartlett, P. F. and Coulson, E. J. (2010). p75 neurotrophin receptor regulates basal and fluoxetine-stimulated hippocampal neurogenesis. *Exp. Brain Res.* **200**, 161-167. doi:10.1007/s00221-009-1947-6

Declercq, J., Brouwers, B., Pruniau, V. P. E. G., Stijnen, P., de Faudeur, G., Tuand, K., Meulemans, S., Serneels, L., Schraenen, A., Schuit, F. et al. (2015). Metabolic and behavioural phenotypes in Nestin-Cre mice are caused by hypothalamic expression of human growth hormone. *PLoS ONE* **10**, e0135502. doi:10.1371/journal.pone.0135502

Delogu, A., Sellers, K., Zagoraiou, L., Bocianowska-Zbrog, A., Mandal, S., Guimera, J., Rubenstein, J. L. R., Sugden, D., Jessell, T. and Lumsden, A. (2012). Subcortical visual shell nuclei targeted by ipRGCs develop from a Sox14+-GABAergic progenitor and require Sox14 to regulate daily activity rhythms. *Neuron* **75**, 648-662. doi:10.1016/j.neuron.2012.06.013

Dubois, N. C., Hofmann, D., Kaloulis, K., Bishop, J. M. and Trumpp, A. (2006). Nestin-Cre transgenic mouse line Nes-Cre1 mediates highly efficient Cre/loxP mediated recombination in the nervous system, kidney, and somite-derived tissues. *Genesis* **44**, 355-360. doi:10.1002/dvg.20226

Englund, C., Fink, A., Lau, C., Pham, D., Daza, R. A., Bulfone, A., Kowalczyk, T. and Hevner, R. F. (2005). Pax6, Tbr2, and Tbr1 are expressed sequentially by radial glia, intermediate progenitor cells, and postmitotic neurons in developing neocortex. *J. Neurosci.* **25**, 247-251. doi:10.1523/JNEUROSCI.2899-04.2005

Erck, C., Meisinger, C., Grothe, C. and Seidl, K. (1998). Regulation of nerve growth factor and its low-affinity receptor (p75NTR) during myogenic differentiation. *J. Cell. Physiol.* **176**, 22-31. doi:10.1002/(SICI)1097-4652(199807)176:1<22::AID-JCP3>3.0.CO;2-A

Gilmore, E. C. and Herrup, K. (1997). Cortical development: layers of complexity. *Curr. Biol.* **7**, R231-R234. doi:10.1016/S0960-9822(06)00108-4

Hamlin, A. S., Windels, F., Boskovic, Z., Sah, P. and Coulson, E. J. (2013). Lesions of the basal forebrain cholinergic system in mice disrupt idiothetic navigation. *PLoS ONE* **8**, e53472. doi:10.1371/journal.pone.0053472

Hashimoto-Torii, K., Motoyama, J., Hui, C.-C., Kuroiwa, A., Nakafuku, M. and Shimamura, K. (2003). Differential activities of Sonic hedgehog mediated by Gli transcription factors define distinct neuronal subtypes in the dorsal thalamus. *Mech. Dev.* **120**, 1097-1111. doi:10.1016/j.mod.2003.09.001

Ibáñez, C. F. and Simi, A. (2012). p75 neurotrophin receptor signaling in nervous system injury and degeneration: paradox and opportunity. *Trends Neurosci.* **35**, 431-440. doi:10.1016/j.tins.2012.03.007

Jenkinson, M., Beckmann, C. F., Behrens, T. E. J., Woolrich, M. W. and Smith, S. M. (2012). Fsl. *Neuroimage* **62**, 782-790. doi:10.1016/j.neuroimage.2011.09.015

Johnston, A. L. M., Lun, X., Rahn, J. J., Liacini, A., Wang, L., Hamilton, M. G., Parney, I. F., Hempstead, B. L., Robbins, S. M., Forsyth, P. A. et al. (2007). The p75 neurotrophin receptor is a central regulator of glioma invasion. *PLoS Biol.* **5**, e212. doi:10.1371/journal.pbio.0050212

Kee, N., Sivalingam, S., Boonstra, R. and Wojtowicz, J. M. (2002). The utility of Ki-67 and BrdU as proliferative markers of adult neurogenesis. *J. Neurosci. Methods* **115**, 97-105. doi:10.1016/S0165-0270(02)00007-9

Kendall, S. E., Goldhawk, D. E., Kubu, C., Barker, P. A. and Verdi, J. M. (2002). Expression analysis of a novel p75(NTR) signaling protein, which regulates cell cycle progression and apoptosis. *Mech. Dev.* **117**, 187-200. doi:10.1016/S0925-4773(02)00204-6

Kerbler, G. M., Hamlin, A. S., Pannek, K., Kurniawan, N. D., Keller, M. D., Rose, S. E. and Coulson, E. J. (2013). Diffusion-weighted magnetic resonance imaging detection of basal forebrain cholinergic degeneration in a mouse model. *Neuroimage* **66**, 133-141. doi:10.1016/j.neuroimage.2012.10.075

Krygier, S. and Djakiew, D. (2002). Neurotrophin receptor p75(NTR) suppresses growth and nerve growth factor-mediated metastasis of human prostate cancer cells. *Int. J. Cancer* **98**, 1-7. doi:10.1002/ijc.10160

Lee, K. F., Bachman, K., Landis, S. and Jaenisch, R. (1994). Dependence on p75 for innervation of some sympathetic targets. *Science* **263**, 1447-1449. doi:10.1126/science.8128229

Liu, C., Li, Y., Edwards, T. J., Kurniawan, N. D., Richards, L. J. and Jiang, T. (2016). Altered structural connectome in adolescent socially isolated mice. *Neuroimage* **139**, 259-270. doi:10.1016/j.neuroimage.2016.06.037

Ma, Y., Hof, P. R., Grant, S. C., Blackband, S. J., Bennett, R., Slatest, L., McGuigan, M. D. and Benveniste, H. (2005). A three-dimensional digital atlas database of the adult C57BL/6J mouse brain by magnetic resonance microscopy. *Neuroscience* **135**, 1203-1215. doi:10.1016/j.neuroscience.2005.07.014

Marin, O., Anderson, S. A. and Rubenstein, J. L. R. (2000). Origin and molecular specification of striatal interneurons. *J. Neurosci.* **20**, 6063-6076. doi:10.1523/JNEUROSCI.20-16-06063.2000

Moscatelli, I., Pierantozzi, E., Camaioni, A., Siracusa, G. and Campagnolo, L. (2009). p75 neurotrophin receptor is involved in proliferation of undifferentiated mouse embryonic stem cells. *Exp. Cell Res.* **315**, 3220-3232. doi:10.1016/j.yexcr.2009.08.014

Nakagawa, Y. and O'Leary, D. D. M. (2001). Combinatorial expression patterns of LIM-homeodomain and other regulatory genes parcellate developing thalamus. *J. Neurosci.* **21**, 2711-2725. doi:10.1523/JNEUROSCI.21-08-02711.2001

Olsson, M., Björklund, A. and Campbell, K. (1998). Early specification of striatal projection neurons and interneuronal subtypes in the lateral and medial ganglionic eminence. *Neuroscience* **84**, 867-876. doi:10.1016/S0306-4522(97)00532-0

Paxinos, G. and Franklin, K. B. J. (2007). The Mouse Brain in Stereotaxic Coordinates, 2nd edn. Elsevier.

Pellow, S., Chopin, P., File, S. E. and Briley, M. (1985). Validation of open:closed arm entries in an elevated plus-maze as a measure of anxiety in the rat. *J. Neurosci. Methods* **14**, 149-167. doi:10.1016/0165-0270(85)90031-7

Pillai, A. G., de Jong, D., Kanatsou, S., Krugers, H., Knapman, A., Heinzmann, J.-M., Holsboer, F., Landgraf, R., Joëls, M. and Touma, C. (2012). Dendritic morphology of hippocampal and amygdalar neurons in adolescent mice is resilient to genetic differences in stress reactivity. *PLoS ONE* **7**, e38971. doi:10.1371/journal.pone.0038971

Pontious, A., Kowalczyk, T., Englund, C. and Hevner, R. F. (2008). Role of intermediate progenitor cells in cerebral cortex development. *Dev. Neurosci.* **30**, 24-32. doi:10.1159/000109848

Qian, L., Milne, M. R., Shepheard, S., Rogers, M.-L., Medeiros, R. and Coulson, E. J. (2018). Removal of p75 neurotrophin receptor expression from cholinergic basal forebrain neurons reduces amyloid-beta plaque deposition and cognitive impairment in aged APP/PS1 mice. *Mol. Neurobiol.* **56**, 4639-4652. doi:10.1007/s12035-018-1404-2

Reichardt, L. F. (2006). Neurotrophin-regulated signalling pathways. *Phil. Trans. R. Soc.* **361**, 1545-1564. doi:10.1098/rstb.2006.1894

Rubenstein, J. L. R., Anderson, S., Shi, L., Miyashita-Lin, E., Bulfone, A. and Hevner, R. (1999). Genetic control of cortical regionalization and connectivity. *Cereb. Cortex* **9**, 524-532. doi:10.1093/cercor/9.6.524

Silva, C. G., Peyre, E., Adhikari, M. H., Tielens, S., Tanco, S., Van Damme, P., Magno, L., Krusy, N., Agirman, G., Magiera, M. M. et al. (2018). Cell-intrinsic control of interneuron migration drives cortical morphogenesis. *Cell* **172**, 1063-1078.e1019. doi:10.1016/j.cell.2018.01.031

Song, H., Lee, B., Pyun, D., Guimera, J., Son, Y., Yoon, J., Baek, K., Wurst, W. and Jeong, Y. (2015). Ascl1 and Helt act combinatorially to specify thalamic neuronal identity by repressing Dlxs activation. *Dev. Biol.* **398**, 280-291. doi:10.1016/j.ydbio.2014.12.003

Takada, M., Fishell, G., Li, Z. K., Van der Kooy, D. and Hattori, T. (1987). The development of laterality in the forebrain projections of midline thalamic cell groups in the rat. *Dev. Brain Res* **35**, 275-282. doi:10.1016/0165-3806(87)90052-6

Tronche, F., Kellendonk, C., Kretz, O., Gass, P., Anlag, K., Orban, P. C., Bock, R., Klein, R. and Schütz, G. (1999). Disruption of the glucocorticoid receptor gene in the nervous system results in reduced anxiety. *Nat. Genet.* **23**, 99-103. doi:10.1038/12703

Ullmann, J. F. P., Watson, C., Janke, A. L., Kurniawan, N. D., Paxinos, G. and Reutens, D. C. (2014). An MRI atlas of the mouse basal ganglia. *Brain Struct. Funct.* **219**, 1343-1353. doi:10.1007/s00429-013-0572-0

Verbeke, S., Meignan, S., Lagadec, C., Germain, E., Hondermarck, H., Adriaenssens, E. and Le Bourhis, X. (2010). Overexpression of p75(NTR) increases survival of breast cancer cells through p21(waf1). *Cell. Signal.* **22**, 1864-1873. doi:10.1016/j.cellsig.2010.07.014

Vilar, M., Murillo-Carretero, M., Mira, H., Magnusson, K., Besset, V. and Ibáñez, C. F. (2006). Bex1, a novel interactor of the p75 neurotrophin receptor, links neurotrophin signaling to the cell cycle. *EMBO J.* **25**, 1219-1230. doi:10.1038/sj.emboj.7601017

von Schack, D., Casademunt, E., Schweigreiter, R., Meyer, M., Bibel, M. and Dechant, G. (2001). Complete ablation of the neurotrophin receptor p75NTR causes defects both in the nervous and the vascular system. *Nat. Neurosci.* **4**, 977. doi:10.1038/nn730

Wiese, C., Rolletschek, A., Kania, G., Blyszczuk, P., Tarasov, K. V., Tarasova, Y., Wersto, R. P., Boheler, K. R. and Wobus, A. M. (2004). Nestin expression–a property of multi-lineage progenitor cells? *Cell. Mol. Life Sci.* **61**, 2510-2522. doi:10.1007/s00018-004-4144-6

Young, K. M., Merson, T. D., Sotthibundhu, A., Coulson, E. J. and Bartlett, P. F. (2007). p75 neurotrophin receptor expression defines a population of BDNF-responsive neurogenic precursor cells. *J. Neurosci.* **27**, 5146-5155. doi:10.1523/JNEUROSCI.0654-07.2007

Yushkevich, P. A., Piven, J., Hazlett, H. C., Smith, R. G., Ho, S., Gee, J. C. and Gerig, G. (2006). User-guided 3D active contour segmentation of anatomical structures: significantly improved efficiency and reliability. *Neuroimage* **31**, 1116-1128. doi:10.1016/j.neuroimage.2006.01.015

Zagrebelsky, M., Holz, A., Dechant, G., Barde, Y. A., Bonhoeffer, T. and Korte, M. (2005). The p75 neurotrophin receptor negatively modulates dendrite complexity and spine density in hippocampal neurons. *J. Neurosci.* **25**, 9989-9999. doi:10.1523/JNEUROSCI.2492-05.2005

Zanin, J. P., Abercrombie, E. and Friedman, W. J. (2016). Proneurotrophin-3 promotes cell cycle withdrawal of developing cerebellar granule cell progenitors via the p75 neurotrophin receptor. *eLife* **5**, e16654. doi:10.7554/eLife.16654

Zhang, W., Zeng, Y.-S., Wang, J.-M., Ding, Y., Li, Y. and Wu, W. (2009). Neurotrophin-3 improves retinoic acid-induced neural differentiation of skin-derived precursors through a p75NTR-dependent signaling pathway. *Neurosci. Res.* **64**, 170-176. doi:10.1016/j.neures.2009.02.010

Zhao, Y., Marin, O., Hermesz, E., Powell, A., Flames, N., Palkovits, M., Rubenstein, J. L. R. and Westphal, H. (2003). The LIM-homeobox gene Lhx8 is required for the development of many cholinergic neurons in the mouse forebrain. *Proc. Natl. Acad. Sci. USA* **100**, 9005-9010. doi:10.1073/pnas.1537759100